Hindawi
Advances in Civil Engineering
Volume 2019, Article ID 8036928, 11 pages
https://doi.org/10.1155/2019/8036928

Research Article

Floor Failure Evolution Mechanism for a Fully Mechanized Longwall Mining Face above a Confined Aquifer

Jinghui Zhai,[1] Danlong Liu,[2] Gang Li,[3] and Fangtian Wang[3]

[1]*Shunhe Coal Mine, Yongcheng Coal & Electricity Holding Group Co., Ltd., Yongcheng 476600, China*
[2]*Chengjiao Coal Mine, Henan Zhenglong Coal Industry Co., Ltd., Yongcheng 476600, China*
[3]*School of Mines, Key Laboratory of Deep Coal Resource Mining, Ministry of Education of China, China University of Mining and Technology, Xuzhou 221116, China*

Correspondence should be addressed to Gang Li; lgang_27@cumt.edu.cn and Fangtian Wang; wangfangtian111@163.com

Received 20 July 2018; Revised 2 October 2018; Accepted 17 December 2018; Published 13 January 2019

Guest Editor: Dengke Wang

In longwall mining, the risk of water inrushes from the floors of deeply buried coal seams is closely related to the degree and depth of the destruction for the mining floor. To analyze the main factors affecting floor failure and the evolution of such failures, this study considered the LW2703 working face of the Chengjiao Coal Mine in China, which is characterized by a large buried depth, complex fault structure, and high pressure from a confined aquifer. The characteristics affecting floor crack development depth were analyzed by considering friction angle, cohesion force, floor pressure, stress increase coefficient, and peak position. A FLAC3D simulation was performed to compare the degrees of floor damage that occurred for caving and backfilling methods during the mining process. High-density electrical detection was performed on-site and used to (1) determine the maximum depth range of the floor damage, (2) reveal the laws governing the evolution of damage in a mining floor, and (3) provide a reasonable basis for evaluating and preventing floor water inrush accidents.

1. Introduction

As Chinese coal mines gradually become deeper, their hydrogeological conditions become increasingly complex. The combination of ground and water pressure has made water damage more prominent and increased the frequency of floor water inrush accidents. Heavy casualties and economic losses, combined with high-frequency growth, have become a critical risk to the safe and efficient operation of coal mines [1, 2]. Figure 1 shows that while water hazard accidents and deaths in coal mines have generally decreased in recent years in China, heavy casualties and economic losses still occur. Therefore, further investigation is needed into the detection and prevention of water hazards in mines.

Floor water inrushing occurs when certain basic conditions are satisfied for a water source and channel. For the north China coalfield, the water source is generally the water-filled aquifer of the Carboniferous and Ordovician systems. This indicates that the safety of a mining face depends mainly on channel formation, which is controlled by many factors. Hidden structure activation leads to water inrushing [3], which indicates that water damage is closely related to the degree and depth of structural damage. Therefore, studying the evolution of mining floor failures is of great theoretical and practical significance.

Many researchers in China and abroad have investigated mining floor failure laws and water inrush controls. Yao et al. [4] presented a suite of fully coupled governing equations to determine fracture erosion and changes in rock permeability. To determine the hydraulic conductivity of a rock formation between a deeply buried coal seam and an aquifer, Huang et al. [5] conducted four water injection tests at the Baodian Coal Mine. Zhai et al. [6] simulated and analyzed the failure characteristics at different depths under fluid-solid coupling conditions to develop a water inrush law. Li et al. [7] used a double scalar D-P elastoplastic

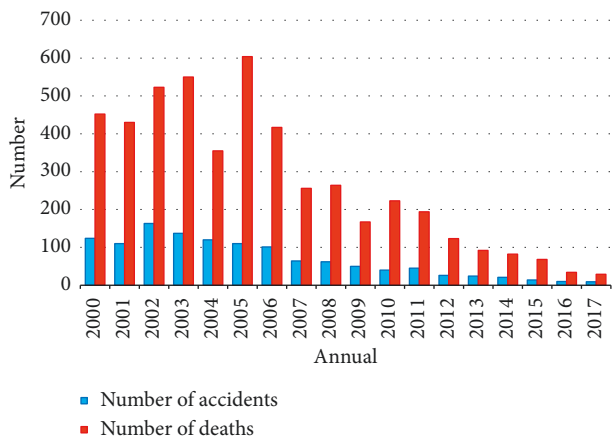

Figure 1: Coal mine water disasters in China between 2000 and 2017.

damage constitutive model to study the evolution of a complete base plate from an aquifer to an aqueduct. Wang [8] analyzed key methods for preventing floor water damage in the Fengfeng mining area and proposed comprehensive prevention and control techniques, such as geophysical exploration and ground grouting reinforcement. Wu et al. [9] systematically classified mine water hazards and provided a basis for their classification and prevention. Chen and Cao [10] analyzed the hydrogeological conditions and karst development rules for karst water in the Pingdingshan Coal Mine, as well as the water-filling conditions of the mine and its karst fissure distribution. Wang et al. [11, 12] performed a Hopkinson pressure bar experiment to study the dynamic failure characteristics of coal and indicated that its dynamic compressive strength was positively correlated with its elastic modulus. Guo et al. [13] divided flooding patterns into three types: complete floor crack extension, primary channel conduction, and concealed structure sliding shear. They studied different modes for the spatiotemporal evolution of water inrush channels.

The LW2703 working face in the Chengjiao Coal Mine is very deep, with a complex fault structure and high water pressure. Because of these characteristics, the face has a high water inrush risk, which threatens safe mining and production. We investigated the LW2703 working face and analyzed how floor crack development depth was affected by friction angle, cohesion force, floor pressure, stress increase coefficients, and peak position. We used a FLAC3D simulation to compare and analyze how caving and backfilling methods affected the degree of floor damage during mining. High-density electrical detection was performed in the field and used to (1) determine the maximum depth of floor damage, (2) reveal the laws governing the evolution of damage in a mining floor, and (3) provide a reasonable basis for evaluating and preventing floor water inrush accidents.

2. Engineering Background

The LW2703 working face of the Chengjiao Coal Mine is located in the seventh mining area of the east wing. The working face has a length of 1043 m along the upper roadway, 926 m along the lower roadway, and 993 m along the middle roadway. The inclined length of the working face is 342.2 m. Figure 2 shows the layout of the working face. The actual exposure during roadway excavation showed that the No. 2 coal seams are stable, with an average coal thickness of 2.8 m, buried depth of over 800 m, and inclination angle of 5°. Figure 3 shows the roof and floor. The floor consists of sandstone and mudstone. The limestone layers below the floor (L_8, L_9, L_{10}, and L_{11}) are rich in aquifers and have low water conductivity, and the cracks in the floor are undeveloped. Instead, the direct water source for the mine is the sandstone in the roof and floor. The indirect water supply source is the limestone in L_{11} and L_{10}. The main water source that threatens the working face is the upper limestone of the Taiyuan Formation. The L_{11} and L_{10} limestone layers are located 74.0 and 63.5 m below the No. 2 coal seam, respectively. The water pressure is 4.2–4.5 MPa. The limestone and No. 2 coal seam have relatively stable mudstone and sandy mudstone phase barriers, and water inrushing is unlikely to occur under normal conditions. However, Mining activities can cause floor damage and crack the floor strata. At the same time, the natural fissures in the lower part of the aquifer develop upwards, which further reduces the thickness of the water-resisting layer and can cause water inrush accidents at the working face.

3. Main Factors Affecting the Degree of Floor Damage

3.1. Factors Affecting Floor Crack Development Depth. The rock strength index has a certain effect on the development of floor cracks. In this work, we analyzed the effects of the floor crack development depth on the internal friction angle, cohesion force, floor pressure, stress increasing coefficient, and peak position were analyzed. The shear stress near the coal wall was high, a condition that can easily cause fissures. The crack depth reached a maximum value within 150 m from the cutting eye and 30 m from the coal wall. Therefore, this zone was selected for the tests and analysis.

3.1.1. Relationship between Internal Friction Angle, Cohesion, and Floor Crack Development Depth. Figure 4 shows fitting curves for the internal friction angle and cohesion, based on tests.

Figure 4(a) shows a positive correlation, which indicates that a larger internal friction angle corresponds to a larger floor crack development depth and vice versa. The two parameters have a power exponential relationship, which can be expressed as follows:

$$h = 3.0926e^{0.2608a}, \quad R^2 = 0.9819, \tag{1}$$

where α is the internal friction angle in the rock body and R^2 is the reliability.

Figure 4(b) shows a linear relationship between crack development depth and cohesion. Crack development depth

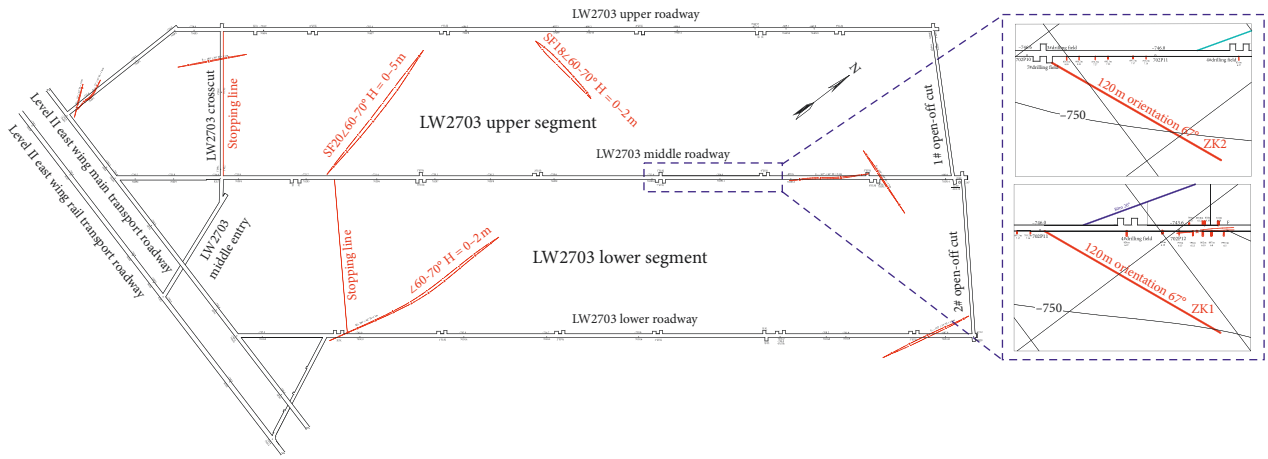

Figure 2: LW2703 working face layout.

increases with cohesion, and this linear relationship can be represented as follows:

$$h = 0.2681C^2 - 0.1742C,\quad R^2 = 0.09963, \tag{2}$$

where C is the cohesion in the rock body (MPa).

3.1.2. Relationship between the Floor Water Pressure and Depth of Floor Crack Development. Changes in the pressure of the confined water influence floor cracks. This can be expressed by the curves shown in Figure 5.

The development depth of the floor cracks increases slowly between confined water pressures of 0 to 2 MPa and then increases rapidly for higher pressures. The floor crack development depths were 10.8 and 17 m at 2 and 3 MPa, respectively, which represents an increase of 57.4%. The depth at 4 MPa was 24 m. The relationship is expressed as follows:

$$h = 0.9571p^2 - 1.2829p + 6.54,\quad R^2 = 0.9976, \tag{3}$$

where P is the water pressure and R^2 is the reliability.

3.1.3. Relationship between Abutment Pressure Concentration Coefficient and Depth of Cracks in the Floor. The floor crack development depth changes with the bearing pressure concentration coefficient, as shown by the curve in Figure 6.

The fissure development depth first decreases and then increases with the concentration coefficient. The concentration coefficient reaches a minimum between 2.5 and 3.5 and is approximately 3, which indicates that the floor crack development depth is shallow. In addition, intersection points 2 and 4 for the actual and fitted curves indicate that the two parameters have an equal effect when the lumping factors are 2 and 4. The linear relationship is expressed as follows:

$$h = 1.525k^2 - 7.563k + 17.85,\quad R^2 = 0.8688, \tag{4}$$

where K is the concentration pressure coefficient.

3.1.4. Relationship between the Peak Position of the Support Pressure and Crack Depth. The continuous advancement of the coal mining face means that the distance between the working surface and peak position of the support pressure is constantly changing. This results in a corresponding change in the crack depth. Figure 7 shows the curve for this relationship.

As the mining face continues to advance, the distance between the location of the peak bearing pressure and the mining face increases, and the floor crack development depth slowly increases before reaching a plateau. At this point, increasing the distance no longer increases the damage and depth. The relationship is expressed as follows:

$$h = 1.1199 \ln L + 6.7277,\quad R^2 = 0.9648, \tag{5}$$

where L is the distance between the mining face and the location of the peak abutment pressure.

3.1.5. Floor Damage Depth Induced by Longwall Mining. As shown in Figure 8, the maximum floor damage depth h_a induced by longwall mining can be calculated with fracture mechanics theory.

The working face is assumed to be a crack in the internal part of an infinite rock. For the working face, the mining thickness is much smaller than the mining width. Consequently, the maximum damage depth h_a in the floor can be calculated as follows [14]:

$$h_a = \frac{1.57\gamma^2 H^2 a (1 - \sin\varphi)^2}{16c^2 \cos^2\varphi}, \tag{6}$$

where γ is the average weight of the overlying coal seam layer (25 kN/m^3), H is the buried depth of the coal seam (846 m), c and φ are the average cohesion (15.8 MPa) and internal friction angle (30°), respectively, for the floor rock, and a is the width of the working face (342.2 m). As a result, the floor damage depth was calculated to be 20.1 m.

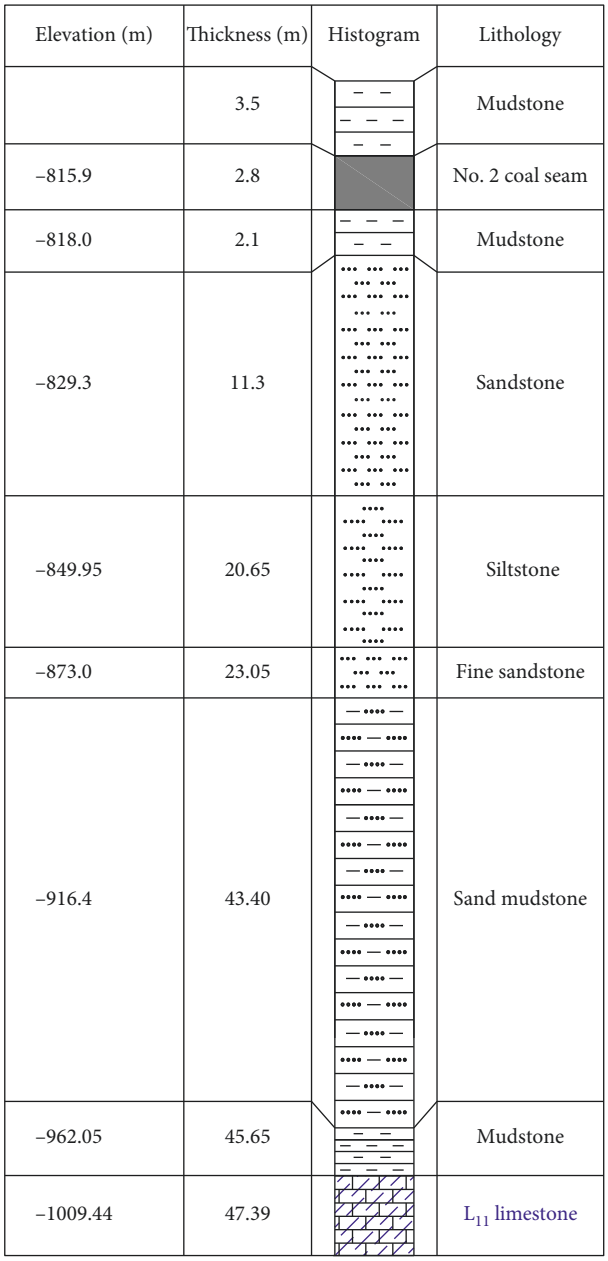

Figure 3: Coal seam histogram.

3.2. Simulation Analysis of the Floor Damage Degree. FLAC3D was used to develop the numerical models for caving and backfilling mining.

3.2.1. Stress Distribution of the Mining Floor. Figure 9 shows the vertical stress contours 2 m below the floor when the working face was advanced by 80, 120, and 160 m. When the roof was controlled with a caving method, the stress in the front and on both sides of the working face increased, and stress in the goaf area decreased. The area of increased stress advanced with the work surface. The maximum stress in front of the working face was 8.5 MPa, which was 1.5 times that of the original rock, and the bearing pressure affected the rock within a range of 35–40 m. Both sides of the working face appear on the change of stress as shown in Figure 10. The vertical stress on the rock formations decreased. The stress in the goaf is gradually recovering as the working face advanced.

When the backfilling method was used, stress concentrations also occurred. The maximum stress was 7.2 MPa, which was 1.2 times the stress of the normal rock. The supporting pressure had a range of 25–30 m, which subsequently decreased as the working face advanced. Rock formations were noted in the goaf area. The reduction in vertical stress was lower than the corresponding reduction for the caving method. This indicates that the backfill transferred part of the stress in the goaf, which gradually changed the surrounding rock stress.

The overall stress distribution characteristics were similar for the caving and backfilling methods; however, the caving method produced a higher degree of stress concentration, while the backfilling method produced a gentler curve for the change in stress.

3.2.2. Distribution of the Plastic Zone in the Mining Floor. Figure 11 shows the distribution of the floor's plastic zone under the midsection of the working face along the strike. As the plastic zone continued to advance, the floor first entered shear plastic yielding and then experienced tensile yield failure. Based on the mine pressure, the depth of the effects can be divided into three zones: direct damage, impact, and minor change.

For the caving method, when the working face advanced 80 m, shear plastic yielding developed to 24 m below the floor, and tensile yielding developed to 6 m. When the working face advanced 80 m, shear yielding still developed to 24 m, but the range increased; the tensile yielding developed to 7 m below the floor, and its range also expanded. When the working face advanced 120 m, the shear yielding did not change, and the range was wider; the tensile yielding developed to 12 m below the floor and no longer developed downward. The range also continued to expand.

For the backfilling method, damage to the floor was greatly reduced, and tensile yielding only occurred around 2 m near the roof and floor. When the working face advanced 80 m, shear yielding developed to 8 m below the floor. When the working face advanced 160 m, shear yielding developed to 11 m. A comparison of the caving and backfilling methods shows that the backfilling method can effectively control failure because the shear yielding depth for backfilling was approximately one-third that for caving.

In summary, different mining techniques caused the stress field and plastic zone to have different development ranges. The caving method causes a greater crack development depth than the filling method and more intense damage to the floor.

4. Exploring the Evolution of Mining-Induced Floor Failures

Compared with traditional drilling methods, high-density resistivity imaging technology is advantageous because it can

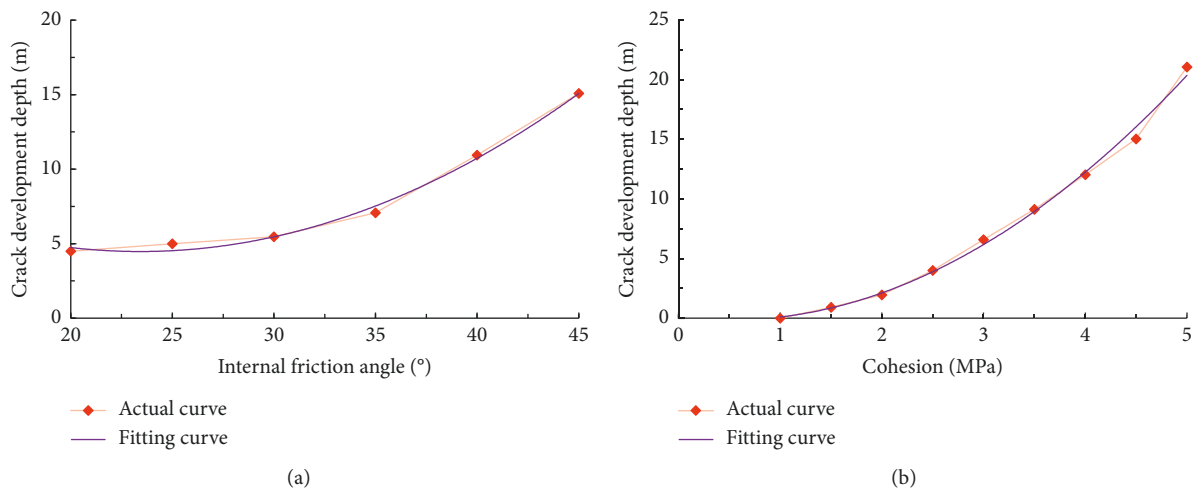

Figure 4: Fitting curves of fracture development depth versus (a) internal friction angle and (b) cohesion.

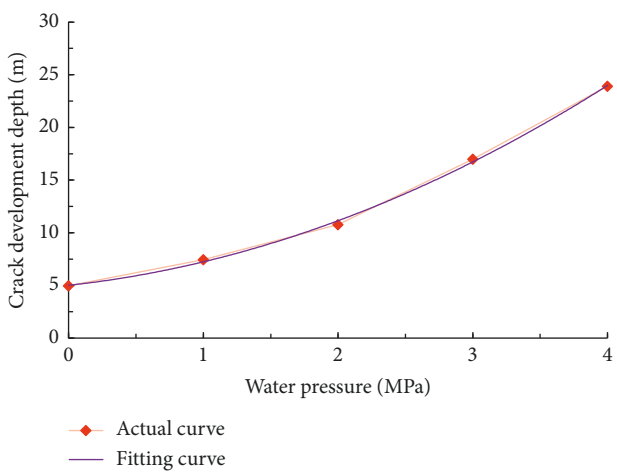

Figure 5: Curve for water pressure and fracture development.

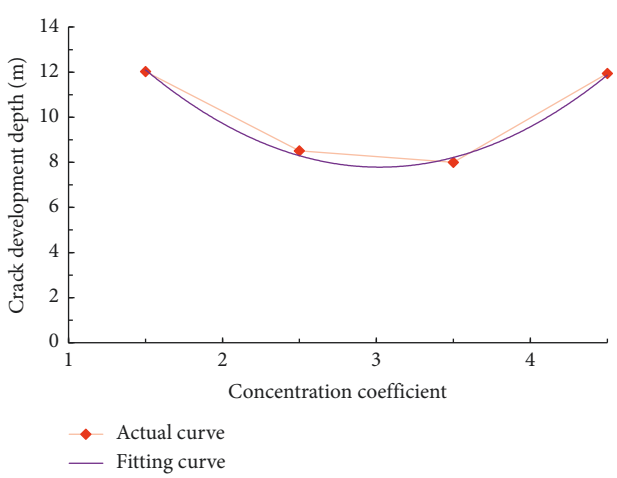

Figure 6: Curve of the accommodating pressure concentration and crack development.

be used efficiently at construction sites; it has a large detection range and can be used to perform continuous and dynamic observations. It is used to obtain the electrical

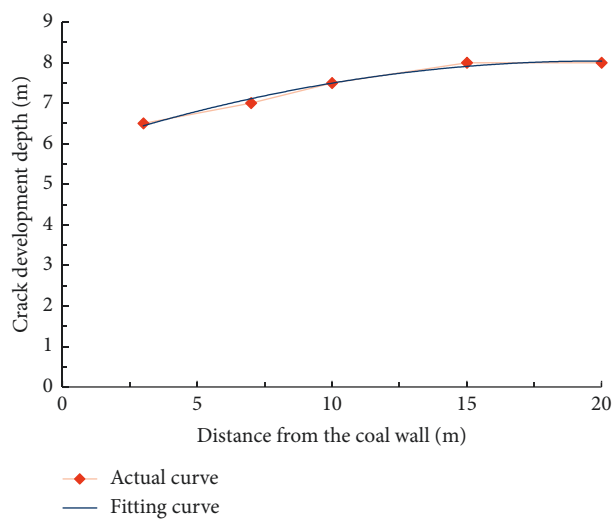

Figure 7: Fitting curve of the crack development depth and support pressure at the floor.

occurrence state of coal seams before and after mining and to intuitively analyze and judge the extent of damage depth of mining. The continuous detection capabilities of high-density resistivity imaging were used to dynamically monitor the LW2703 working face to study the damage rules and failure depth of the working face floor.

We adopted a system using the WDJD-3 high-density electric method. This system has a large storage capacity, performs accurate and fast measurements, is convenient to operate, and is easy to use with domestic high-density electrical processing software, which makes interpretation more convenient and intuitive.

4.1. Drilling Arrangement. Borehole #1 was drilled at 713 m along the LW2703 middle roadway, with a drilling orientation of 67°, a drilling inclination of −35°, and a drilling length of 120 m. Borehole #2 was drilled at 640 m along the

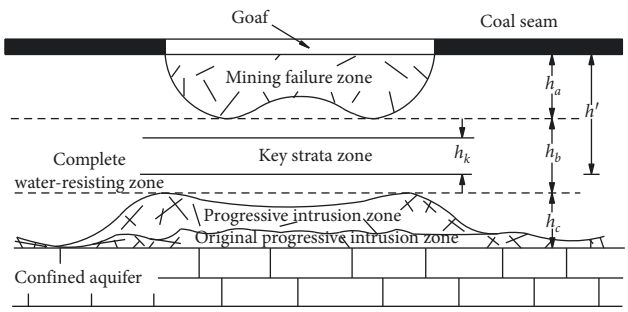

Figure 8: Depth of the mining failure of the floor.

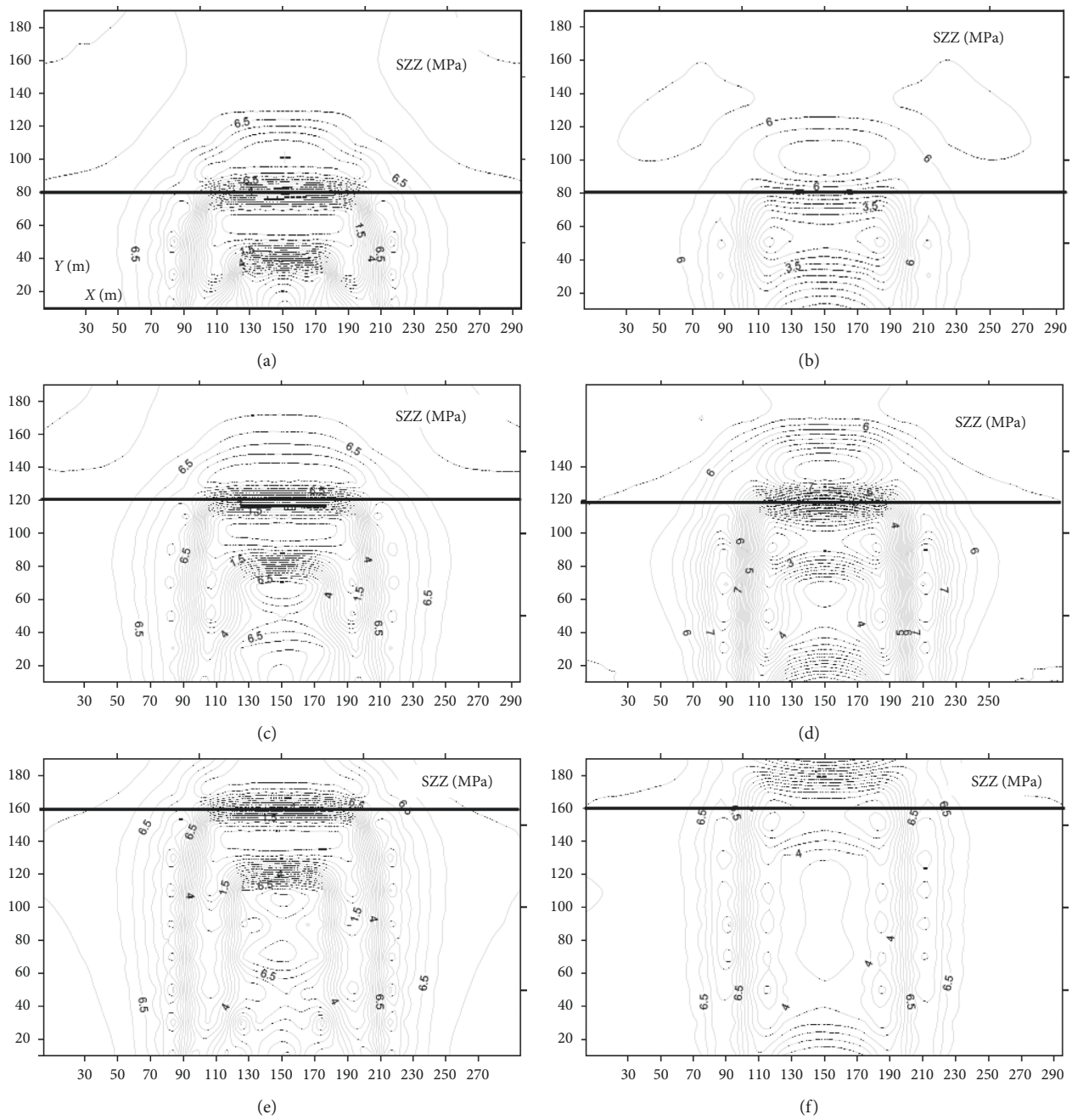

Figure 9: Vertical stress of the floor at different advance distances: 80 m mining advance by (a) caving and (b) backfilling; 120 m mining advance by (c) caving and (d) backfilling; and 160 m mining advance by (e) caving and (f) backfilling.

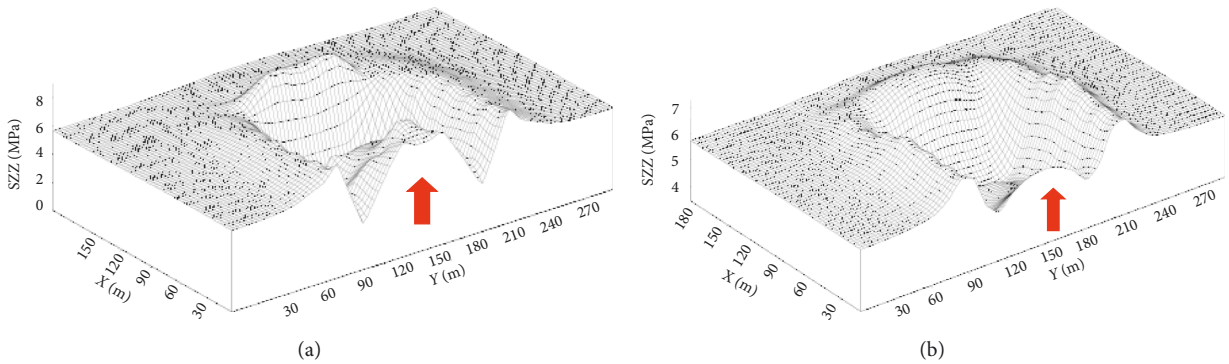

Figure 10: Stress perspective for a 120 m mining advance: (a) caving and (b) backfilling.

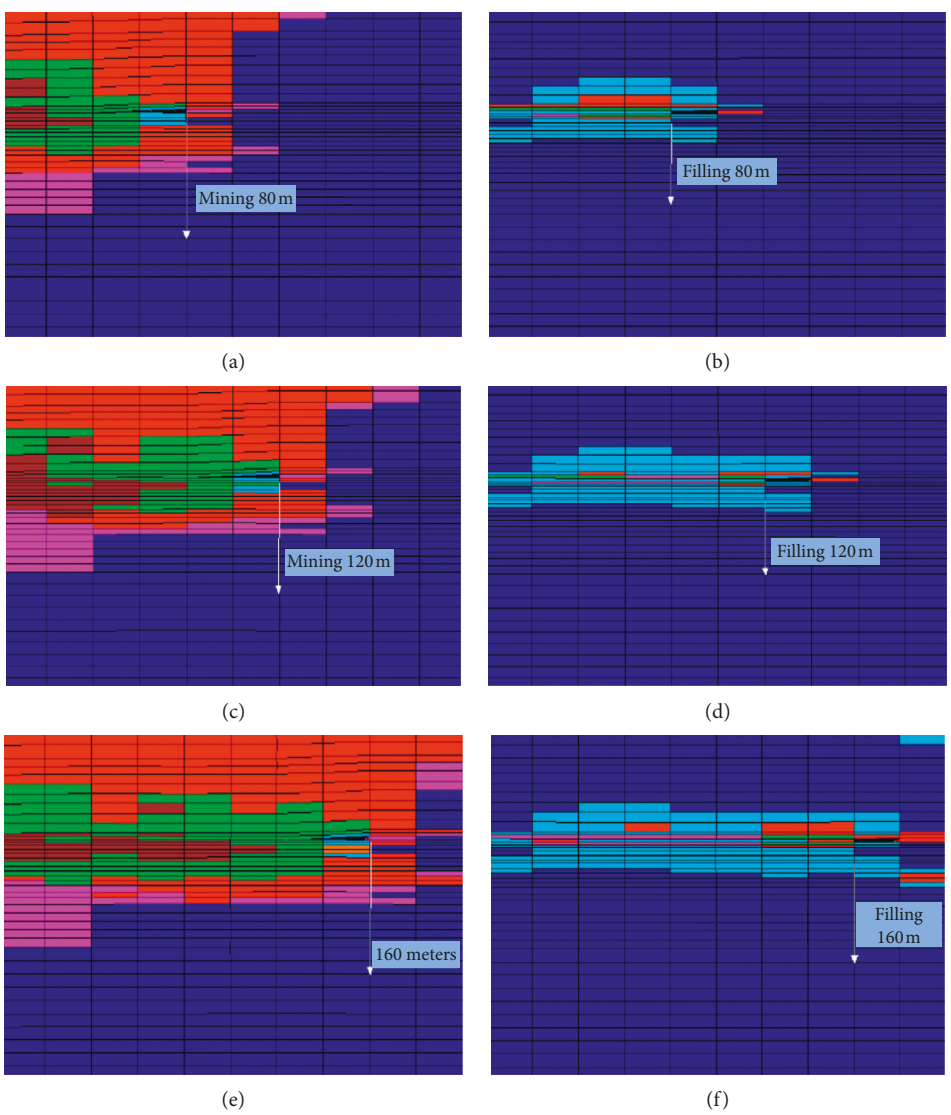

Figure 11: Development range of the plastic zone for the floor at different advance distances: 80 m mining advance by (a) caving and (b) backfilling; 120 m mining advance by (c) caving and (d) backfilling; and 160 m mining advance by (e) caving and (f) backfilling.

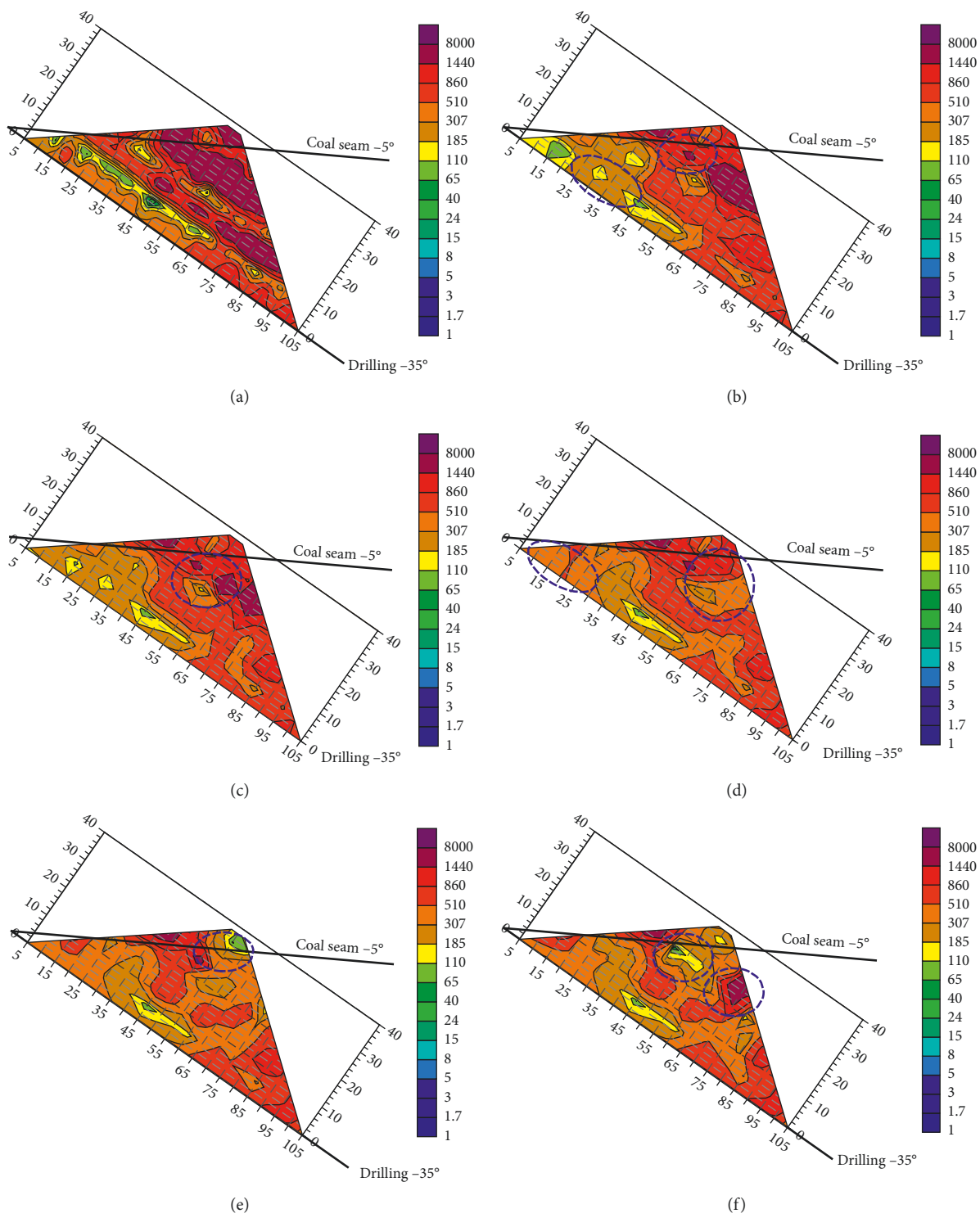

Figure 12: Continued.

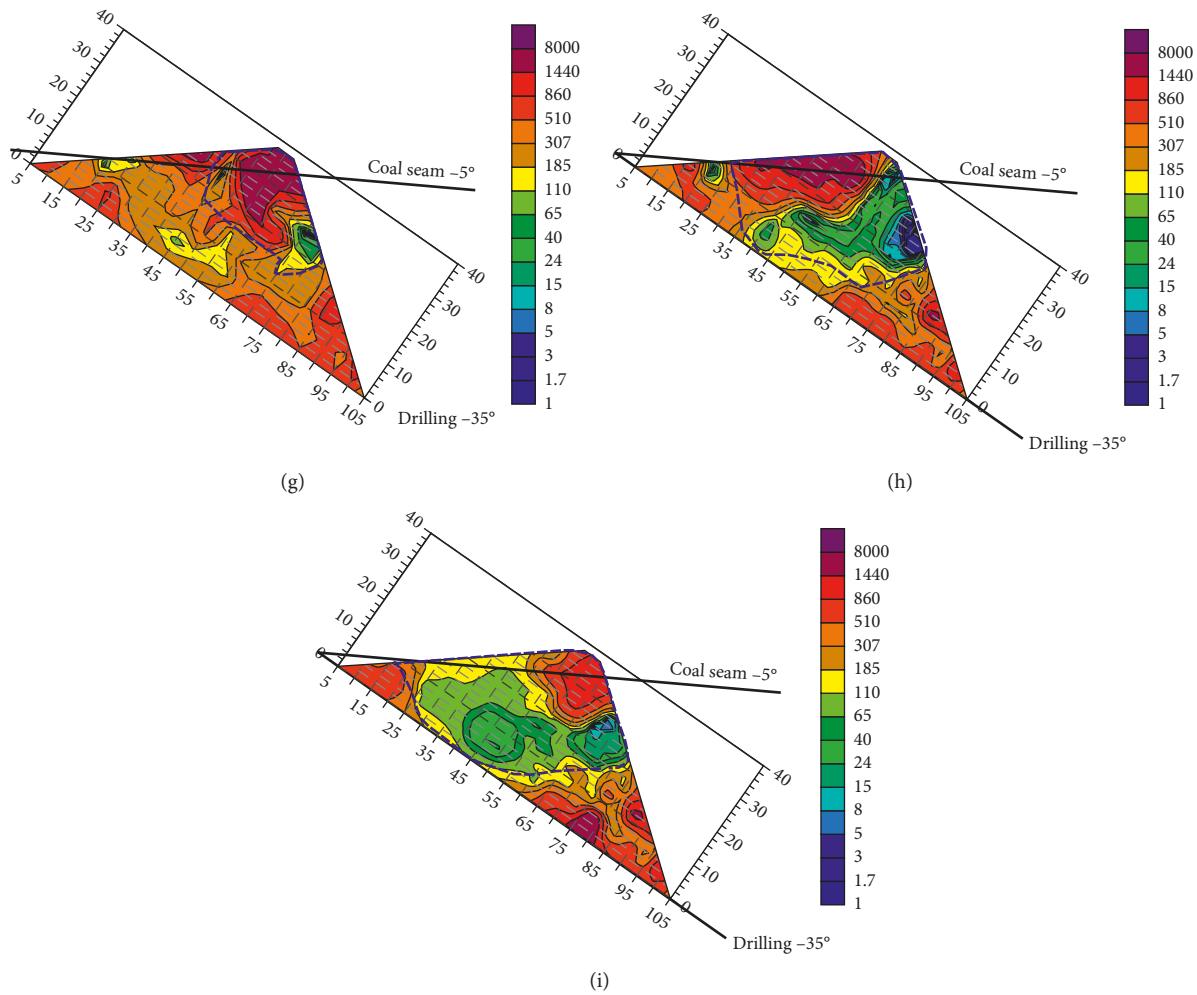

Figure 12: Resistivity results for borehole #1 at different locations on the working face: (a) 814 m, (b) 807 m, (c) 802 m, (d) 796 m, (e) 793 m, (f) 783 m, (g) 762 m, (h) 682 m, and (i) 557 m.

middle roadway of LW2703, with the same drilling parameters used for borehole #1. The layout is shown in Figure 2.

4.2. Results Analysis of the Borehole #1 Resistivity. Figure 12 shows the resistivity detection results for borehole #1 at different locations. Changes in the apparent resistivity are indicated by colors; red indicates high apparent resistivity and blue indicates low apparent resistivity. The thick blue dotted line shows the difference relative to the previous detection. A total of 29 electrodes were used to perform measurements; the electrodes were spaced 4 m apart. A-MN-B (α) and MN-B devices were used for detections. Comparative tests showed that the α device had a large detection area, good stability, and high sensitivity to subtle electrical changes. The detection results for the α device are explained in the remainder of this section. Table 1 presents the parameters for borehole #1 at different stopping locations.

Multiple explorations of the two boreholes, combined with the exploration map and the geological conditions of the working face, revealed the following:

(1) Multiple comparisons showed obvious electrical changes, and the rules governing these changes were in good agreement with the theoretical characteristics. In particular, the results for borehole #1 were relatively stable, and the data were accurate and reliable.

(2) In the early stages of drilling, when the water or slurry in the hole was not solidified, a low-resistance screening effect was clearly detected. As the slurry gradually solidified, electrode grounding gradually improved. The detection data gradually approached the electrical characteristics of the formation.

(3) In the early stages of the rock formation destruction at the working face, the rock layer was broken, the size of cracks increased, resistivity increased sharply, there was high disorder, and the destruction depth was shallow. As the working face continued to advance, the failure depth of the floor rock layer gradually increased. The gradual filling of sandstone pores and fissures with water caused resistivity to decrease sharply. The apparent resistivity fell below 100 Ω·m.

Table 1: List of detection parameters.

No.	Mining position (m)	Detection results
1	814	The electrical characteristics are chaotic, and low resistance characteristics appear near the borehole.
2	807	Two obvious electrical changes: (1) a 20–45 m hole depth and a 0–10 m vertical distance to the borehole; (2) a 40–60 m hole depth, a 20–30 m vertical distance to borehole, and a 0–5 m vertical distance to coal seam floor.
3	802	One obvious electrical change: a 45–65 m hole depth, an approximately 15–30 m vertical distance to the borehole, and an approximately 0–14.3 m vertical distance to the coal seam floor.
4	796	Two obvious electrical changes: (1) 5–30 m hole depth, 0–10 m vertical distance to drill hole, and 0–14 m vertical distance to floor; (2) 50–70 m hole depth, 15–35 m vertical distance to drill hole, and about 0–17 m vertical distance to coal floor.
5	793	One obvious electrical change: a 45–65 m hole depth, a 20–40 m vertical distance to the drill hole, and a 0–5.2 m vertical distance to the floor.
6	783	Two obvious electrical changes: (1) at a hole depth of 45–55 m, the location of the work water and the greater grounding of the metal body led to a significant reduction; (2) at a 60–75 m hole depth, resistivity was significantly higher than that previously measured. The resistance value suddenly changes from 100 Ω·m to 1000 Ω·m. Based on the mining conditions, it is judged that the floor is broken due to the mining effect. There was no water in the initial stage or slight water cutting. The characteristics of the rock formation clearly were highly electrical.
7	762	One obvious electrical change: a 45–80 m hole depth, a 12–40 m vertical distance to the drill hole, and a 0–24.6 m offset distance from the coal floor. The site was judged to be the floor rock layer destroyed by mining.
8	682	One obvious electrical change: a 25–80 m hole depth. The site was judged to be the floor destroyed by mining.
9	557	Within the same range as the previous change, the rock formation in the initial stage was severely broken by mining. It gradually became compact and stable. The resistance was generally low. There was a certain degree of water absorption, and the distribution was more uniform.

(4) The floor of the detection location was severely broken after mining; it gradually became compact and stable, with low resistance. There was some degree of water absorption, but the distribution rules were relatively uniform, and the shallow part gradually moved from very high to medium resistance with increasing depth to form a wide range of layers of low resistance.

(5) The destruction depth of this exploration mainly focused on borehole #1. The deepest change position occurred at a hole depth of 65 m, with a vertical distance of 6 m from the drill hole and 27.3 m from the coal seam.

5. Conclusions

(1) The LW2703 working face has a relatively complex geology. The limestone in the upper part of the Taiyuan Formation is the main source of water threatening the safety of the working face. This limestone has a water pressure of 4.2–4.5 MPa.

(2) The floor damage depth is related to the floor rock formation lithology in terms of the development degree. The floor rock mass strength index was used to analyze how the friction angle, cohesion force, floor pressure, stress increase coefficient, and peak position affected floor crack development depth.

(3) FLAC3D was used to simulate the stress field and plastic zone development associated with caving and backfilling methods. The caving method produces deeper cracks and more intense floor damage than the filling method.

(4) High-density electrical surveys indicated that the floor damages and the fractured rock formations occur induced by mining effect. In the initial period, there was no or little water present. The electrical characteristics of the rock formations were significantly stronger, and the maximum depth of the floor damage proved the mining floor failure evolution rule.

Data Availability

The data used to support the findings of this study are available from the corresponding author upon request.

Conflicts of Interest

The authors declare that there are no conflicts of interest regarding the publication of this paper.

Acknowledgments

This work was supported by the National Key R&D Program of China (no. 2018YFC0604701), the National Science Foundation for Post-doctoral Scientists of China (no. 2018M630634), the visiting scholarship funded by the China Scholarship Council (no. 201802180034), and the Priority Academic Program Development of Jiangsu Higher Education Institutions. The authors gratefully acknowledge the financial support of the above-mentioned agencies.

References

[1] H. P. Xie, H. W. Zhou, D. J. Xue, H. W. Wang, R. Zhang, and F. Guo, "Research and consideration on deep coal mining and critical mining depth," *Journal of China Coal Society*, vol. 37, no. 4, pp. 535–542, 2012.

[2] F. P. Cui, Q. Wu, Y. H. Lin, and Y. F. Zeng, "Prevention and control techniques and methods for water disasters at coal mines in China," *Journal of Mining Science and Technology*, vol. 3, no. 3, pp. 219–228, 2018.

[3] J. C. Niu, J. L. Zhang, Y. H. Ding, B. L. Wang, and S. Y. Zhu, "Simulation on deformation and failure characteristics of mining floor at deep double-longwall face," *Safety in Coal Mines*, vol. 47, no. 3, pp. 182–186, 2016.

[4] B. Yao, Z. Chen, J. Wei, T. Bai, and S. Liu, "Predicting erosion-induced water inrush of karst collapse pillars using inverse velocity theory," *Geofluids*, vol. 2018, Article ID 2090584, 18 pages, 2018.

[5] Z. Huang, Z. Jiang, S. Zhu, Z. Qian, and D. Cao, "Characterizing the hydraulic conductivity of rock formations between deep coal and aquifers using injection tests," *International Journal of Rock Mechanics and Mining Sciences*, vol. 71, pp. 12–18, 2014.

[6] X. R. Zhai, J. W. Wu, H. M. Zhang, S. H. Shen, and N. C. Tian, "Study on water-inrush mechanism of mining floor of deep coal seam in mine shaft based on fluid-solid coupling," *Coal Science and Technology*, vol. 45, no. 6, pp. 170–175, 2017.

[7] H. Li, H. B. Bai, J. J. Wu et al., "Study on the influence of mechanical properties of rock mass cyclic loading and unloading on the evolution of the intact floor," *Chinese Journal of Rock Mechanics and Engineering*, vol. 37, no. S1, pp. 3470–3480, 2018.

[8] D. L. Wang, "Study on the control techniques about water disaster in deep mines of Fengfeng mine," *Coal and Chemical Industry*, vol. 40, no. 9, pp. 83–85, 2017.

[9] Q. Wu, F. P. Cui, and S. Q. Zhao, "Type classification and main characteristics of mine water disasters," *Journal of China Coal Society*, vol. 38, no. 4, pp. 561–565, 2013.

[10] X. M. Chen and S. K. Cao, "Prevention and control technology of high pressure karst water from Permo-Carboniferous seam floor," *Coal Science and Technology*, vol. 46, no. 3, pp. 182–187, 2018.

[11] D. K. Wang, S. M. Liu, J. P. Wei, H. L. Wang, and M. Peng, "Analysis and strength statistical damage constitutive model of coal under impacting failure," *Journal of China Coal Society*, vol. 41, no. 12, pp. 3024–3031, 2016.

[12] D. K. Wang, S. M. Liu, J. P. Wei, B. H. Yao, and M. Peng, "The failure characteristics of coal under impact load in laboratory," *Journal of Mining & Safety Engineering*, vol. 34, no. 3, pp. 594–600, 2017.

[13] W. J. Guo, S. C. Zhang, W. B. Sun, and J. T. Chen, "Experimental and analysis research on water finrush catastrophe mode from coal seam floor in deep mining," *Journal of China Coal Society*, vol. 43, no. 1, pp. 219–227, 2018.

[14] J. C. Zhang, Y. Z. Zhang, and T. Q. Liu, *Rock Mass Permeability and Coal Mine Water Inrush*, Geological Publishing House, Beijing, China, 1997.